Sustainable Energy & Fuels

ROYAL SOCIETY OF CHEMISTRY

PAPER

View Article Online
View Journal | View Issue

Cite this: *Sustainable Energy Fuels*, 2024, **8**, 2235

Comparing a covalently linked BODIPY–pyrene system *versus* the corresponding physical mixture as chromophores in luminescent solar concentrators†

Massimiliano Cordaro,[ab] Giulia Neri,[a] Anna Piperno,[a] Ambra M. Cancelliere,[a] Antonio Santoro,[a] Scolastica Serroni,[a] Francesco Nastasi[ac] and Antonino Arrigo *[ac]

Luminescent solar concentrators (LSCs) appear as an attractive solution to extend the application of photovoltaic panels by installing them "invisibly" in urban architectures. Many researchers are working on boosting the photovoltaic performances of LSCs, and an appealing strategy is to involve a multichromophoric system where Förster resonance energy transfer (FRET) occurs. To investigate the role of the energy donor, which is crucial in FRET processes inside LSCs, we designed a light-harvesting antenna composed of a highly emissive donor, such as pyrene, covalently connected to a BODIPY unit as an energy acceptor. Such an antenna was used as the chromophore to fabricate a LSC and the photovoltaic performance of the device was compared with that of the LSC based on a physical mixture of BODIPY and pyrene not covalently bonded. The results indicate that the LSC based on the antenna system has a lower optical efficiency than the LSC containing the physical mixture. Such a conclusion highlights that designing an antenna system composed of a highly luminescent species as the energy donor (*e.g.* pyrene, in this case) could not improve the LSC photovoltaic performances compared to the LSC based on the physical mixture of the separated chromophores.

Received 9th March 2024
Accepted 7th April 2024

DOI: 10.1039/d4se00329b

rsc.li/sustainable-energy

Introduction

Over the recent years, renewable energies are progressing as valuable options to replace conventional energy sources based on fossil fuels, which are causing climate and environmental issues on the planet.[1–5] Among the existing sustainable technologies, such as wind, biomass or hydroelectric, solar energy conversion appears to be one of the most attractive considering that during one hour the Sun provides to the Earth's surface a quantity of energy approximately equal to the energy consumed in the globe over one year.[6,7] In the last few decades, various solar energy conversion devices have been developed, including photovoltaic (PV) panels which achieve outstanding conversion efficiencies. Although the use of photovoltaics has been recently diffused globally, nowadays less than 1% of our total energy consumption is generated by this technology;[8] such an assessment suggests that the installation of more PV panels is necessary, but on the other hand, this would include covering some habitable landscapes, implying environmental and strategic consequences.[9] A possible solution to extend the PV applications in large areas is the development of building integrated photovoltaics (BIPVs), where energy-generating technologies are installed into architectural structures.[10] In this context, luminescent solar concentrators (LSC), proposed for the first time in 1973,[11] appear as a praiseworthy solution. LSCs are transparent plastic or glass materials containing luminophores which absorb a portion of the solar spectrum and emit photons at lower energy. Due to the high refraction index of the LSC matrix which causes a total internal reflection phenomenon, the luminescence is waveguided to the edges of the material, where photovoltaic panels are mounted and convert emitted photons into electrical energy.[12–15] LSCs can be applied in a series of urban architectures, for instance in noise barriers,[16–18] greenhouses,[19] and bus stops,[20] or used as windows, thus "invisibly" incorporating the PV panels in the buildings, without altering the indoor illumination and helping the diffusion of photovoltaic technologies on large areas.[21]

Various luminophores have been tested inside LSCs, such as quantum dots (QDs) or molecules.[22–25] Luminescent QDs are nanomaterials exhibiting a notable photo-stability in liquid and solid states and a large Stokes-shift which avoids emission

[a]*Department of Chemical, Biological, Pharmaceutical and Environmental Sciences, University of Messina, Viale Ferdinando Stagno d'Alcontres, 31, 98166 Messina, Italy*
[b]*ITAE-CNR, Via Salita S. Lucia Sopra Contesse 5, Messina, Italy*
[c]*Interuniversitary Research Center for Artificial Photosynthesis (Solar Chem, Messina Node), V. F. Stagno d'Alcontres 31, 98166 Messina, Italy*

† Electronic supplementary information (ESI) available: Materials and methods adopted; synthetic procedures and characterization; spectroscopic data; LSC preparations; data on photovoltaic investigations. See DOI: https://doi.org/10.1039/d4se00329b

losses due to re-absorption phenomena.[26,27] Nevertheless, the highest values of power conversion efficiencies for a LSC-PV coupled system have been reached by using luminescent molecular dyes, like the case of the record value obtained by using up-conversion dual panel LSCs containing a porphin–palladium complex and a perylene unit.[28,29]

Although a large number of fascinating chromophores have been explored for LSC applications, using a single chromophoric species leads to a material capable of absorbing only a limited portion of the solar spectrum. To overcome such a limit, an appealing approach is to construct a covalently linked multi-chromophoric system composed of a chromophore (*i.e.* donor) which absorbs light and funnels the excitation energy to a luminophore (*i.e.* acceptor) which emits photons.[30] Such systems behave as a light-harvesting antenna where Förster resonance energy transfer (FRET) processes occur.

The concept of FRET and an antenna system entrapped in the LSC matrix was introduced in 1977,[31] with the goal to fabricate a LSC capable of absorbing a wider part of the solar spectrum and in parallel to improve the optical properties of the material and mitigate the energy losses in the LSC.[32–36]

In the last few years, several research groups studied the energy transfer process as a possible strategy to boost the efficiency of LSC-PV devices, and the results highlighted that the selection of an appropriate energy donor and an acceptor is a crucial feature for designing an efficient antenna system.[37–39] In particular, it is well acknowledged that an appropriate donor must have a strong absorption in the visible region; however, less attention is typically dedicated to its luminescence properties.

Focusing specifically on the role of the donor in FRET, here we report on a LSC based on a series of BODIPY (difluoroBOronDIPYrromethene) derivatives, including a species (named **Bod-Py**, see Fig. 1) where a pyrene unit is covalently linked to the BODIPY "core", through an amide bond of aliphatic and aromatic spacers. The excited singlet state of pyrene lies at a higher energy compared to the excited singlet state of BODIPY, which favours the BODIPY–pyrene system to behave like an antenna, where the pyrene unit plays the role of the energy donor and the BODIPY moiety, the role of the energy acceptor and emitter. BODIPY and pyrene derivatives have impressive photophysical properties, such as strong visible absorption and remarkable luminescence quantum yield, which make such chromophores to be employed in a plethora of applications,[40–45] including solar energy conversion.[46,47]

Here, the photophysical investigations on the synthetized species and the photovoltaic performances of LSCs are presented. In particular, the optical efficiency of the LSC based on **Bod-Py** was compared with that of the LSC based on the physical mixture of the chromophores that are notcovalently connected, spotlighting the effect of choosing a highly luminescent species (*i.e.* pyrene) as the energy donor in these systems.

Results and discussion

Synthesis and photochemical characterization in solution

The molecular species **Bod-NH$_2$** and **Bod-Amide** (Fig. 1), used as models, were synthesized according to known procedures.[48]

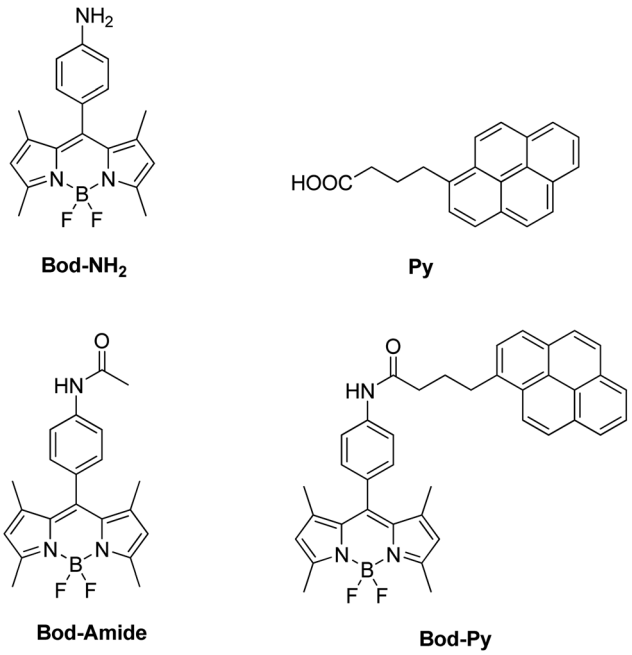

Fig. 1 Molecular structures of the synthetized BODIPY derivatives and pyrene.

Bod-Py was synthesized by a coupling reaction between **Bod-NH$_2$** and commercial 1-pyrenebutyric acid **Py**. Experimental data are provided in the ESI.†

The steady state photophysical properties of these species have been studied in dichloromethane (DCM) dilute solutions ($\sim 10^{-6}$ M) and are summarized in Table 1 and illustrated in Fig. 2 (and the ESI†).

The absorption spectrum of **Py** shows a series of bands in the UV region reflecting the vibronic structure of the $\pi \rightarrow \pi^*$ transitions (as typical for polycyclic aromatic units) with a maximum at 339 nm. The absorption spectra of **Bod-NH$_2$** and **Bod-Amide** are essentially identical to one another and show a dominant band in the visible region attributable to $S_0 \rightarrow S_1$ ($\pi \rightarrow \pi^*$) transitions, and less intense bands in the UV region due to $S_0 \rightarrow S_2$ transitions. **Bod-Py** exhibits an absorption spectrum which corresponds to the overlay of **Bod-Amide** and **Py** bands, indicating that the electronic coupling between BODIPY and pyrene subunits is negligible at the ground state.

In a fluid solution, **Py** has a luminescence quantum yield of 13%, with an emission band maximum centred at 395 nm, and an excited state lifetime of 32 ns. The emission spectra of **Bod-NH$_2$** and **Bod-Amide** show a narrow band with a maximum centred at 510 nm and 512 nm, respectively; it is worth noting that the luminescence quantum yield of **Bod-NH$_2$** is lower than that of **Bod-Amide** (Table 1) and this is due to the presence of an amino group in **Bod-NH$_2$** which partially quenches the BODIPY excited stated fluorescence *via* non radiative decay pathways compared to **Bod-Amide**, where such an effect is downsized. As further confirmation, the excited state lifetime of **Bod-NH$_2$** is shorter that that of **Bod-Amide**. In the emission spectrum of **Bod-Py**, after excitation in the absorption region of pyrene, the BODIPY fluorescence band is exclusively observable, indicating

Table 1 Photophysical data of the studied species in DCM aerated solution and in a LSC rigid matrix

		λ_{max} (nm) absorption		λ_{max} (nm) emission		τ (ns)		
	ε (M^{-1} cm^{-1})	In DCM	In LSC	In DCM	In LSC	In DCM	In LSC	φ in DCM
Py	33 000	339	340	395	396	32	202	0.13
Bod-NH$_2$	73 000	496	498	510	516	2.3	5.8	0.32
Bod-Amide	71 300	497	498	512	516	3.2	6.3	0.40
Bod-Py	73 000	340[a], 497[b]	341[a], 498[b]	512	515	3.6	6.4	0.41
Mix[c]	—	339[a], 497[b]	340[a], 498[b]	395[a], 513[b]	396[a], 517[b]	3.9[a], 32[a,b]	6.6[a,b], 198[a,b]	—

[a] Band maximum or lifetime related to the pyrene unit. [b] Band maximum or lifetime related to the BODIPY unit. [c] The mixture composed of **Bod-Amide** and **Py** in a ratio of 1 : 1 is named **Mix**; see the text.

that **Py** emission is completely quenched *via* a quantitative energy transfer mechanism, where excitation energy migrates from ***Py** to the BODIPY "core" subunit. This is confirmed by the excitation spectrum of **Bod-Py** which quite well matches the corresponding absorption spectrum (Fig. S4, in ESI†). Moreover, data in Table 1 indicate that covalently connecting a pyrene moiety to BODIPY does not affect φ and τ of **Bod-Py** compared to those of **Bod-Amide** (taken as "model" species), as expected in systems where energy transfer processes take place.[31] A similar BODIPY–pyrene dyad, connected by one phenyl unit as the spacer, had been investigated by M. Fakis *et al.* and it was demonstrated that not only the energy transfer process, but also the photoinduced electron transfer process takes place in the dyad when a polar solvent is employed.[49–51] To avoid such a process which would quench the luminescence, we decided to use an aliphatic chain as the linker between the chromophoric units in order to decrease the electronic coupling between BODIPY and pyrene compared to a conjugated spacer, thus making the charge separation process less competitive.

By using the Förster equation,[17] we calculated the rate constant of the energy transfer mechanism occurring in **Bod-Py**:

$$k_{en}^{F} = 8.8 \times 10^{-25} \frac{K^2 \Phi}{r_{AB}{}^6 n^4 \tau} J_F \quad (1)$$

where K is an orientation factor which considers the directional nature of the dipole–dipole interaction and K^2 is typically 2/3 for a random orientation; n is the refractive index of the solvent (DCM); φ and τ are respectively the luminescence quantum yield and lifetime of the energy donor (**Py** in our case) in DCM solution; r_{AB} is the distance in Å between pyrene and BODIPY units in **Bod-Py** (*i.e.* approximately 9.6 Å); J_F is the Förster overlap integral between the emission spectrum of the donor (*i.e.* **Py**) and the absorption spectrum of the acceptor (*i.e.* **Bod-Amide**) on an energy scale in cm^{-1} (in our case, J_F = 1.77×10^{-14} cm^6 $mmol^{-1}$). According to eqn (1), k_{en}^{F} for **Bod-Py** in DCM is 1.35×10^{10} s^{-1} which is much faster than the rate constant of **Py** excited state radiative decay, that is 3.16×10^{7} s^{-1}, indicating that the Förster energy transfer

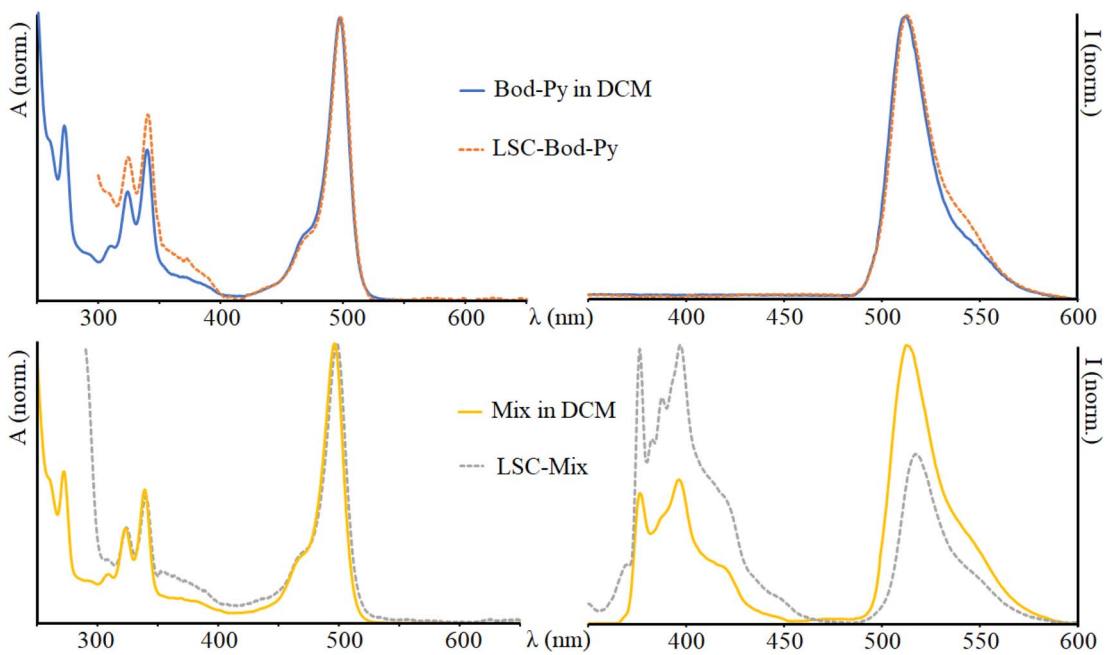

Fig. 2 Absorption (on the left) and emission (on the right) spectra of **Bod-Py** and **Mix** in DCM and in the LSC. λ_{exc} = 350 nm. The spectra of the other species are illustrated in the ESI.†

process is kinetically a competitive process which quenches **Py** luminescence.

As a control sample, a physical mixture (meaning a mixture of distinct molecular entities of donor and acceptor units) composed of **Bod-Amide** and **Py** in a ratio of 1 : 1 has been prepared in DCM dilute solution (concentration ranging from 1 × 10^{-6} M to 8 × 10^{-6} M), here named **Mix**. The absorption spectrum of **Mix** is identical to that of **Bod-Py**, while the emission spectrum (excitation in the region where pyrene absorbs) reveals the emission band of the pyrene unit, together with the fluorescence band of the BODIPY unit at lower energy. Additionally, the excited state lifetime of pyrene in **Mix** is equal to that of **Py**; furthermore, the excitation spectrum of **Mix** (λ_{em} = 535 nm) perfectly matches the absorption spectrum of **Bod-Amide**, with no contribution of pyrene bands (Fig. S5 in the ESI†). This demonstrates that in the physical solution **Mix**, no energy transfer process occurs, probably because it is diffusion-dominated at this low concentration. Indeed, energy transfer efficiency is inversely proportional to the distance between the donor and the emitter,[52] meaning that, when they are not covalently bonded, quite a high concentration of chromophores is needed for the energy transfer to occur. As an example, for the case of the diffusion-controlled Förster energy transfer mechanism, the concentration of the emitter should be >1 mM in solution to sufficiently quench the donor emission.[53] However, at high concentration values, aggregation phenomena play a key role and can lead to luminescence quenching or enhancement (*i.e.* AIE, aggregation induced emission). In our case, when a π-conjugated system such as pyrene is involved which undergoes π–π stacking interactions, the high concentration of the luminophore required for the energy transfer process can be responsible for aggregation phenomena that have a counter-effect to quench pyrene's luminescence. To avoid such quenching events, we used diluted solutions (∼10^{-6} M) for measurements in the liquid phase and in LSCs.

LSC preparation and optical characterization

LSCs were fabricated by a thermal activated polymerization, where lauryl methacrylate acted as the monomer, ethyl glycol dimethacrylate as the cross-linking agent, and lauroyl peroxide as the initiator,[54] and such a reaction mixture was used to dissolve the synthetized species and **Mix.** All the LSCs have been prepared using the same concentration of chromophores, to allow for a comparison; adopting 10^{-6} M as the concentration range of the chromophore in the LSC was a good compromise for having enough chromophores to generate a performant device and at the same time keeping the LSC transparent and only slightly coloured. The LSC fabrication procedure was repeated several times, using different concentrations of BODIPY or pyrene (from 2.2 × 10^{-6} M to 8 × 10^{-6} M, meaning the chromophore : initiator ratio was from 1 : 8000 to 1 : 2200 respectively), and detecting always the same photochemical results, on the basis of absorption and emission properties. At temperatures higher than 80 °C, the initiator is activated and starts a radical polymerization reaction which leads to a polyacrylic solid material. Investigations on the optical properties and Monte Carlo ray tracing simulations demonstrated that conventional polyacrylates absorb less light than standard window glasses,[55] and this makes them a suitable material for LSC applications.

The prepared LSC appears transparent and exhibits BODIPY's (or pyrene's) fluorescence from the borders once irradiated by UV light from the top surface (except for **LSC-Py**), as shown in Fig. 3.

Comparing the absorption spectra of all the chromophores in the LSC matrix and in DCM solution, no significant difference is noted (just 1 nm red-shift in the LSC matrix compared to the liquid phase).

To calculate the fraction of photons absorbed by the LSC over the solar spectrum from 370 nm to 1050 nm, $\eta_{abs\text{-}vis}$, an AM 1.5G solar simulator was used as the irradiation source. The area of AM 1.5G spectra decreased by the presence of the LSCs between the light source and the detector was divided by the area of the solar spectrum. The $\eta_{abs\text{-}vis}$ values are reported in Table 2 (and graphically observable in Fig. 4 and S6 in the ESI†). For the "blank" LSC (*i.e.* a LSC without a chromophore inside) the fraction of photons absorbed is 12.13%, and it is related to some incident sunlight confined in the waveguide of the polyacrylic rigid matrix. The value of $\eta_{abs\text{-}vis}$ for **LSC-Py** is lower compared to that of the other materials and similar to the value of the blank LSC; this is not surprising considering that the absorption contribution of pyrene in this investigation range (from 370 nm to 1050 nm) is negligible.

As information on the visual appearance of the semi-transparent slab, we calculated the color rendering index (CRI), reported in Table 2, and the color coordinates using the CIE 1931 chromaticity diagram (see Fig. 4, ESI† for details),[56] that are widely investigated parameters to understand the suitability of LSCs in real world BIPV applications. The CRI value of **LSC-Py** is similar to that of **LSC-Blank**, since a pyrene unit is only absorbing the UV portion of the solar spectrum; analogously, the CRI of **LSC-Bod-Py** is almost identical to that of

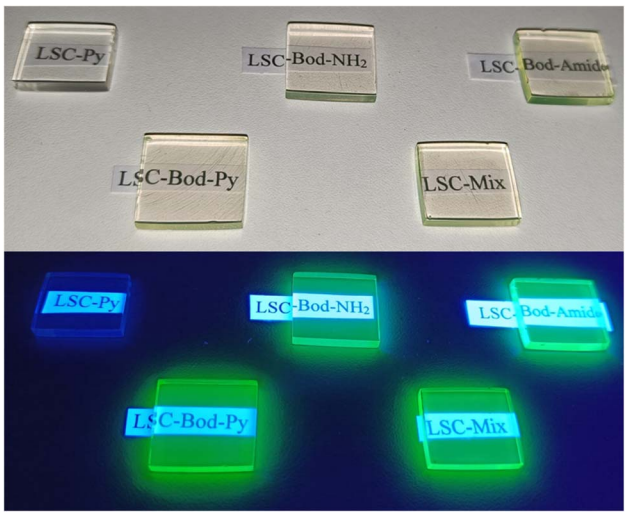

Fig. 3 Photograph of the prepared LSC before and after UV irradiation at 365 nm.

Table 2 Fraction of photons absorbed over the solar spectrum, color coordinates and CRI of the fabricated LSCs

LSC	$\eta_{abs\text{-}vis}$ (%)	x	y	CRI
Blank	12.13	0.337	0.349	96.40
Py	12.56	0.338	0.350	96.05
Bod-NH$_2$	21.62	0.344	0.348	94.45
Bod-Ammide	21.75	0.346	0.348	93.03
Bod-Py	25.75	0.346	0.349	93.05
Mix	25.27	0.348	0.348	91.98

LSC-Bod-Amide. The color coordinates of all the LSCs are located essentially in the central region of the diagram, demonstrating soft coloration of the materials, which is typically a preferable feature for indoor and outdoor illumination. Average visible transmission (AVT) and *La*b** coordinates were also calculated and are included in the ESI.†

Once entrapped in the LSC matrix, the emission maximum of BODIPY derivatives is red-shifted and the luminescence lifetime increases (approximately doubles) compared to that of the solution phase (see Table 1 and Fig. 2). The emission spectrum of **LSC-Bod-Py** does not show pyrene luminescence, thus indicating that the energy transfer mechanism takes place in the solid matrix. The emission spectrum of **LSC-Py** exhibits the same bands of **Py** in DCM; however, the luminescence is strongly enhanced in the rigid phase, as demonstrated by the excited state lifetime which is longer in the LSC (202 ns) compared to the liquid solution (32 ns). This behavior is attributed to the rigid matrix effects which decrease the non-radiative rate constants, thus increasing the excited state lifetime and in parallel enhancing the luminescence quantum yield.[57–59] Such a trend is further confirmed by measuring **Py** luminescence at 77 K in the mixture ethanol : methanol (ratio 4 : 1) rigid matrix, where the fluorescence lifetime decay is 360 ns.

Comparing the emission spectrum of **Mix** in DCM and in LSC at equivalent concentration and under excitation at the same wavelength, it is evident that in the liquid phase the BODIPY luminescence is more intense than pyrene emission, while in the LSC matrix the fluorescence band of the pyrene moiety appears more intense than that of the BODIPY unit. This can be explained considering the boosted luminescence quantum yield of **Py** once in the solid state.

As LSC devices are designed to be exposed to continuous sunlight irradiation, a typical experiment is the photostability test. All the LSCs have been irradiated on the top surface by using an AM 1.5G solar simulator (100 mW cm^2) for 24 h, whilst registering the emission spectra.[60] Despite a mild decrease for an irradiation time longer than 12 hours, the LSC-chromophores fabricated demonstrate adequate stability (Fig. 5).

Photovoltaic performances

To measure the photocurrent generated by the LSC-PV device, one edge of the LSC had been placed in direct contact with a silicon photovoltaic panel and irradiated perpendicularly at 100 mW cm^2 using an AM 1.5G solar simulator,[61,62] while the other borders of the LSC were left uncovered. To reduce the contribution of diffused light to the photocurrent, the PV cell was covered with black tape, leaving exposed only the portion necessary for contact with the LSC. Adopting such an experimental set-up, the short-circuit current intensity, I, (mA) was measured and converted into short-circuit current density J_{LSC} (mA cm^{-2}), dividing I by the area of the LSC in contact with the PV cell ($J = I/A$). Similarly, the short-circuit current density (mA cm^{-2}) of the PV cell, J_{PV}, was obtained by dividing the current intensity by the area of the PV cell directly irradiated by using an AM 1.5G solar simulator (J_{PV} = 15.85 mA cm^{-2} in our case).[63] The so-detected J values, reported in Table 3, were used to calculate the optical efficiency η_{opt} of the LSC-PV, defined by using eqn (2):[64]

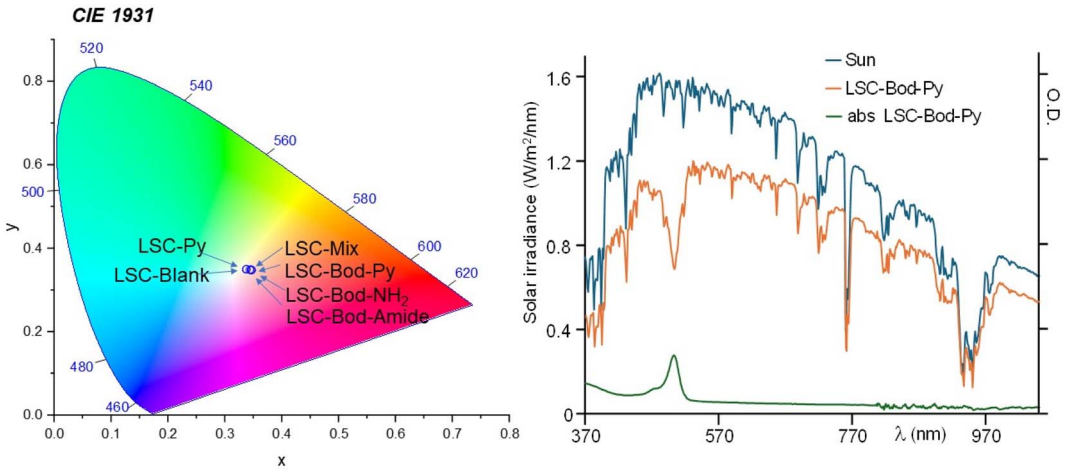

Fig. 4 In the left panel: position of the fabricated LSCs in the CIE 1931 chromaticity diagram. In the right panel: in blue, the solar spectrum using an AM 1.5G filter; the orange line represents the transmission spectrum of the solar simulator filtered by **LSC-Bod-Py**; the absorption spectrum of **LSC-Bod-Py** is shown in green. **LSC-Bod-Py** is selected here as a representative example. The spectra of the other prepared LSCs are illustrated in Fig. S6 in the ESI.†

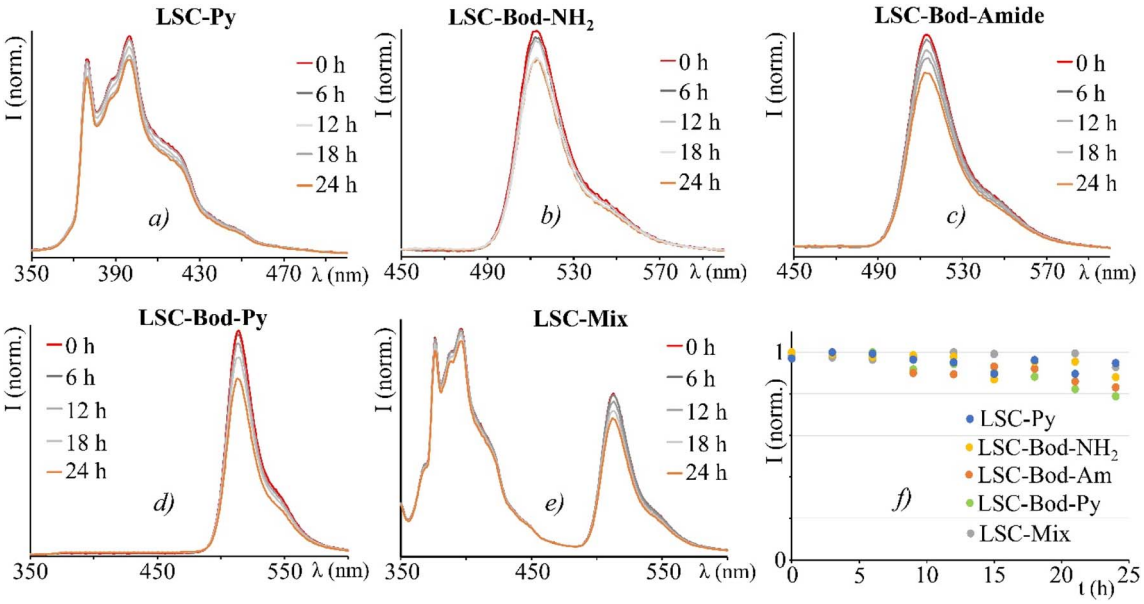

Fig. 5 Panels (a), (b), (c), (d) and (e) show emission spectra (λ_{exc} = 330 nm) of the studied chromophores in the LSC after 24 h of irradiation with a AM 1.5G solar simulator. In panel (f): normalized trend of the luminescence intensities of the corresponding emission band maximum.

Table 3 Photovoltaic data of all the LSCs fabricated, including **LSC-Blank**. The results reported are average values of three experiments. The concentration of chromophores has been the same in all the LSCs to allow for the comparison

LSC	I (mA)	J_{LSC} (mA cm^{-2})	G factor	η_{opt} %	$\eta_{opt\ abs}$ (%)
Blank	0.31 (±0.01)	0.47 (±0.02)	1.29 (±0.01)	2.31 (±0.13)	—
Py	0.72 (±0.01)	1.16 (±0.02)	1.2 (±0.01)	6.14 (±0.19)	—
Bod-NH$_2$	0.66 (±0.01)	1.06 (±0.02)	1.37 (±0.01)	4.88 (±0.15)	51.42
Bod-Amide	0.75 (±0.01)	1.27 (±0.02)	1.42 (±0.01)	5.64 (±0.15)	58.63
Bod-Py	0.75 (±0.01)	1.26 (±0.02)	1.41 (±0.01)	5.67 (±0.15)	41.63
Mix	0.8 (±0.01)	1.52 (±0.03)	1.37 (±0.01)	6.98 (±0.18)	53.12

$$\eta_{opt} = \frac{J_{LSC}}{J_{PV} \times G} \quad (2)$$

where G is a geometrical factor, defined by using eqn (3):[65]

$$G = \frac{A_{top}}{2A_{edge\ long} \times 2A_{edge\ short}} \quad (3)$$

where A_{top} is the area of the top surface of the LSC; $A_{edge\ long}$ and $A_{edge\ short}$ are the areas of the long and short edges of the slab, respectively (the dimensions and contact areas of the LSC are illustrated in Table S1 in the ESI†). In the case of a large LSC, the J_{LSC} value is expected to be typically higher than that for a smaller LSC. The purpose of the G factor is to counterbalance this effect; however, the influence of G and J_{LSC} on η_{opt} is not linear moving from a small to a large LSC. As a matter of fact, generally, the optical efficiency mildly decreases as the G factor increases until reaching a plateau, and this can be attributed to re-absorption events or light losses from the escape cone which more frequently occur in larger LSCs than in smaller ones.[66]

The optical efficiencies, summarized in Table 3, demonstrate adequate performance of LSC-PV devices compared to that of other LSCs based on organic dyes.[67] The results highlight that the η_{opt} of **LSC-Bod-NH$_2$** is lower than that of **LSC-Bod-Amide**, as expected considering that **Bod-NH$_2$** is a less emissive species than **Bod-Amide**, for the reasons discussed above. The optical efficiency of **LSC-Bod-Amide** is almost the same as that of **LSC-Bod-Py**, in agreement with the luminescence quantum yield which is not influenced by the presence of pyrene in the molecular structure. **LSC-Py** exhibits a higher η_{opt} compared to the LSC based on the synthetized BODIPY derivatives, and this can be explained considering the rigid matrix effect which enhances the luminescence of pyrene compared to that in the solution phase, as is evident looking at the excited state lifetimes (Table 1). **LSC-Mix** has the best performance among the series, reaching a η_{opt} value of around 7% that is higher than that of **LSC-Bod-Py**.

A plausible reason for such results could be attributed to the energy transfer process occurring in **LSC-Bod-Py** which quenches pyrene's luminescence, and consequently the photons emitted by only the BODIPY unit contribute to the photocurrent generated from the LSC-PV device. Differently, in **LSC-Mix**, the energy transfer from ***Py** to the BODIPY unit does not take place, and therefore, pyrene is strongly emissive. As a consequence, the photons emitted by both chromophores in **LSC-Mix** (*i.e.* pyrene and BODIPY) contribute to the photocurrent, leading to a better photovoltaic performance compared to that of **LSC-Bod-Py** where only one chromophore (*i.e.* BODIPY) emits light.

Some incident light can follow the LSC waveguide thus contributing to the photocurrent of the LSC-PV device. In order to consider such a contribution, the optical efficiency of the **LSC-Blank** has been calculated and this value (2.31% in our case) can be subtracted from the η_{opt} of all the prepared LSCs, in order to obtain the real optical efficiency ($\eta_{opt\ real}$) of the LSC-PV device, that is: 3.83% for **LSC-Py**, 2.57% for **LSC-Bod-NH$_2$**, 3.33% for **LSC-Bod-Amide**, 3.38% for **LSC-Bod-Py**, and 4.67% for **LSC-Mix**.

Since the η_{opt} value strongly depends on the dimension of the LSC and the chromophore luminescence, we calculated the corrected optical efficiency $\eta_{opt,abs}$ to also consider the fraction of photons absorbed by the LSC-chromophore, according to eqn (4).

$$\eta_{opt\ abs}\ \% = \frac{\eta_{opt}}{\eta_{abs\text{-}vis\ (LSC\text{-}chromophore)} - \eta_{abs\text{-}vis\ (BLANK)}} \quad (4)$$

where $\eta_{abs\text{-}vis\ (LSC\text{-}chromophore)}$ is the fraction of photons absorbed by every LSC containing various chromophores (see Table 2), and $\eta_{abs\text{-}vis\ (BLANK)}$ is the fraction of photons absorbed by **LSC-Blank**. According to this equation, the corrected optical efficiencies are reported in Table 3; for **LSC-Py** $\eta_{opt,abs}$ was not calculated because of the negligible fraction of photons absorbed in the solar spectrum range adopted.

To investigate whether the photocurrent is affected by the position of the irradiation light on the top surface, we measured the *I* value when the light spot of a laser (at 406 nm) is moved from one edge to another of the LSC side. The results are illustrated in Fig. 6, together with the set-up adopted to perform the experiment. The short circuit current intensity for **LSC-Py** is low because **Py** has a low absorption coefficient at the laser irradiation wavelength 406 nm. It is observable that in a LSC based on BODIPY dyes, the photocurrent decreases for a short optical path (meaning the distance between the laser spot on the LSC top surface and LSC border), and then tends towards a plateau. Theoretically, the luminescence intensity reaching the edges should not be influenced by the optical path, which means that the photocurrent should not be altered when the irradiation light is moved from one edge to the other of the slab top surface. In reality, re-absorption events and bulk defects cause the loss of some emitted photons when the optical path is extended, and consequently, the photocurrent slightly decreases.

The incident photon conversion efficiency (IPCE) of the LSC-PV device was obtained by measuring the photocurrent as a function of the excitation wavelength. To perform this experiment, the LSC was placed in contact with the PV cell introduced in the sample compartment of a spectrofluorometer. The IPCE has been calculated according to eqn (5):[68–71]

$$\mathrm{IPCE}\ \% = \frac{(J_{LSC} - J_{LSC\text{-}Blank}) \times 1240}{\lambda \times P_{in}} \quad (5)$$

where J_{LSC} is the current density of the LSC containing the chromophore; $J_{\mathbf{LSC\text{-}Blank}}$ is the current density of the LSC matrix; 1240 is a numerical factor which includes the contributions by Planck's constant (6.62×10^{-34} J s), the speed of light (3.0×10^{8} m s^{-1}) and the electronic charge (1.69×10^{-19} C); λ is the excitation wavelength expressed in nm; P_{in} is the optical power density of the lamp source, expressed as mW cm^{-2} and measured every 5 nm wavelength in the spectral range from 400 nm to 650 nm. As evident from Fig. 7, the IPCE spectra have the same profiles as the absorption spectra, thus confirming that the main contribution to the photocurrent is attributed to the chromophores entrapped in the LSCs and not to scattered light waveguided in the matrix.[72] For instrumentation limits related to the power meter used (see the ESI†), it was not possible to measure the current intensity upon excitation at an energy higher than 400 nm. As a consequence, the IPCE of **LSC-Py** is close to 0%, because pyrene does not absorb in the investigated spectral region (400–650 nm). For the same reason, **LSC-Mix** exhibits almost identical IPCE to that of **LSC-Bod-Amide**, as the contribution of pyrene is negligible. Additionally **LSC-Bod-Amide** and **LSC-Bod-Py** (which have similar optical efficiency values), show almost the same IPCE

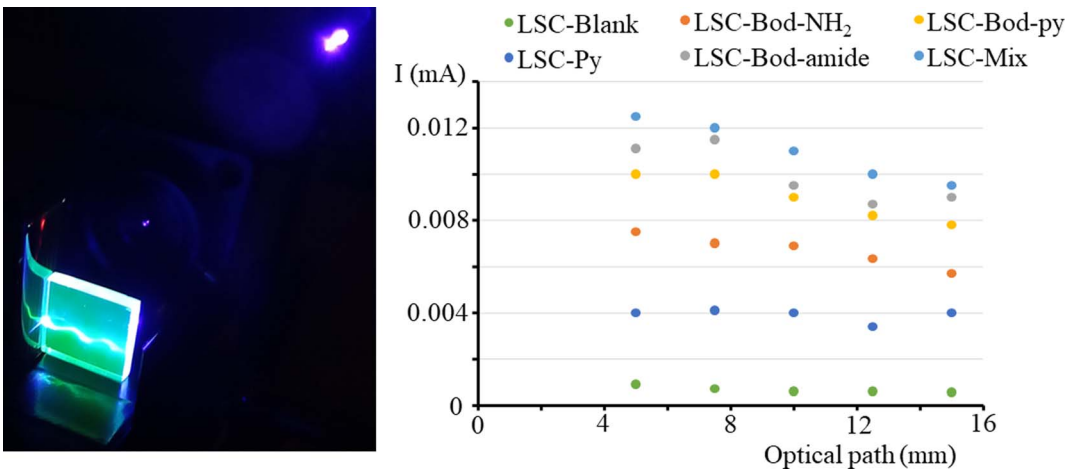

Fig. 6 In the left panel: photograph of the experimental set-up used for monitoring the photocurrent *vs.* optical path; a 406 nm laser is irradiating **LSC-Bod-Py** and the emission light waveguide inside the LSC matrix is visible. In the right panel: diagram illustrating the influence of the optical path on the photocurrent of the LSC-PV device.

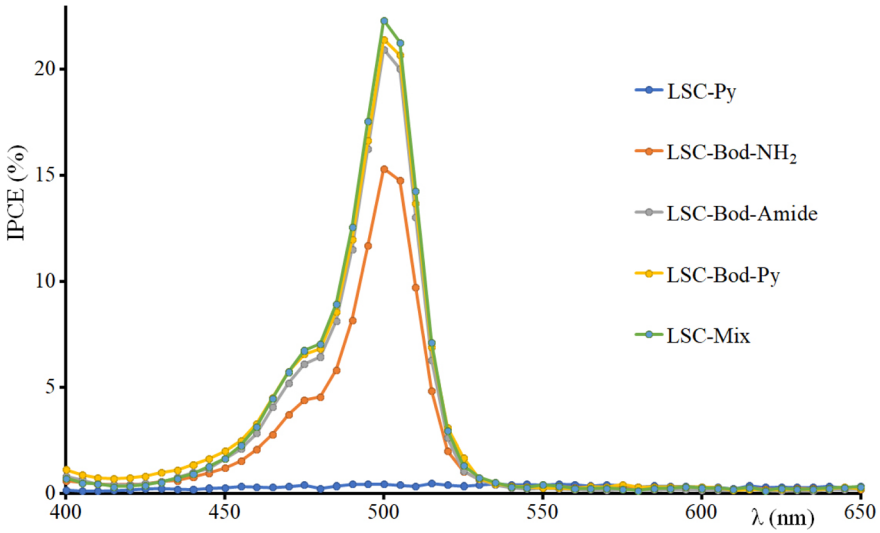

Fig. 7 IPCE spectra of the fabricated LSC.

contribution, in accordance with the photophysical properties of these species.

Conclusions

A series of chromophores (essentially a pyrene moiety and three BODIPY derivatives) have been synthetized, including a species having a pyrene unit covalently connected to the to the BODIPY "core" (named **Bod-Py**). Such chromophores were used to fabricate LSCs which appear transparent and slightly coloured and display the fluorophore's bright luminescence from the edges. Photophysical investigations in the liquid and solid state had been performed, and photovoltaic performances are discussed. In our case, the results highlight that the LSC based on the antenna system **Bod-Py** (where the chromophores are bonded each other) has a lower optical efficiency that the LSC based on the physical mixture (**Mix**) composed of the BODIPY unit and pyrene (not covalently bonded) at the same concentration.

This can be explained considering that in **LSC-Bod-Py** the donor's (pyrene) luminescence is quenched *via* an energy transfer process, so only BODIPY's fluorescence is responsible for the photocurrent generated by the device, while in **LSC-Mix**, both luminophores (BODIPY and pyrene units) contribute to the LSC photocurrent, because non-radiative decay pathways are limited by the donor–acceptor distance and consequently less efficient.

Such results suggest that when a strongly emissive species (like pyrene in our case) is chosen as the energy donor to design an antenna system, the LSC based on the covalently linked donor–acceptor system (where only the acceptor is emissive) would not be more efficient than the LSC based on the physical mixture of the donor and acceptor (where both species emit light). Differently, a good strategy to boost the LSC photovoltaic properties can be to choose a weak-emissive energy donor in order to design an antenna system for a LSC where two (or more) species are covalently bonded, benefitting a wide absorption of the solar spectrum by multiple chromophores and having the excitation energy to be funnelled towards the highly luminescent acceptor.

Conflicts of interest

There are no conflicts of interest to declare.

Acknowledgements

This work was funded by the European Union (NextGeneration EU), through the MUR-PNRR project SAMOTHRACE (ECS00000022).

References

1 N. Armaroli, V. Balzani and N. Serpone, *Powering Planet Earth. Energy Solutions for the Future*, Wiley-VCH, Weinheim, 2013.
2 T. J. Meyer, M. V. Sheridan and B. D. Sherman, *Chem. Soc. Rev.*, 2017, **46**, 6148–6169.
3 D. K. Dogutan and D. G. Nocera, *Acc. Chem. Res.*, 2019, **52**, 3143–3148.
4 S. Campagna, F. Nastasi, G. La Ganga, S. Serroni, A. Santoro, A. Arrigo and F. Puntoriero, *Phys. Chem. Chem. Phys.*, 2023, **25**, 1504–1512.
5 J. Gong, C. Li and M. R. Wasielewski, *Chem. Soc. Rev.*, 2019, **48**, 1862–1864.
6 I. Statistics, *Key World Energy Statistics*, International Energy Agency, France, 2014.
7 R. Eisenberg and D. G. Nocera, *Inorg. Chem.*, 2005, **44**, 6799–6801.
8 E. C. Garnett, B. Ehrler, A. Polman and E. Alarcon-Llado, *ACS Photonics*, 2021, **8**, 61–70.
9 L. Zdražil, *et al.*, *ACS Appl. Energy Mater.*, 2021, **4**, 6445–6453.

10 J. Huang, J. Zhou, E. Jungstedt, A. Samanta, J. Linnros, L. A. Berglund and I. Sychugov, *ACS Photonics*, 2022, **9**, 2499–2509.
11 J. S. Batchelder, H. Zewai and T. Cole, *Appl. Opt.*, 1979, **18**, 3090–3110.
12 B. Petter Jelle, C. Breivik and H. Drolsum Røkenes, *Sol. Energy Mater. Sol. Cells*, 2012, **100**, 69–96.
13 B. S. Richards and I. A. Howard, *Energy Environ. Sci.*, 2023, **16**, 3214–3239.
14 H. Hernandez-Noyola, D. H. Potterveld, R. J. Holt and S. B. Darling, *Energy Environ. Sci.*, 2012, **5**, 5798–5802.
15 J. L. Banal, B. Zhang, D. J. Jones, K. P. Ghiggino and W. W. H. Wong, *Acc. Chem. Res.*, 2017, **50**(1), 49–57.
16 M. Kanellis, M. M. de Jong, L. Slooff and M. G. Debije, *Renewable Energy*, 2017, **103**, 647–652.
17 M. G. Debije, C. Tzikas, V. A. Rajkumar and M. M. de Jong, *Renewable Energy*, 2017, **113**, 1288–1292.
18 M. G. Debije, C. Tzikas, M. M. de Jong, M. Kanellis and L. H. Slooff, *Renewable Energy*, 2018, **116**, 335–343.
19 C. Corrado, S. W. Leow, M. Osborn, I. Carbone, K. Hellier, M. Short, G. Alers and S. A. Carter, *J. Renewable Sustainable Energy*, 2016, **8**, 043502.
20 M. Vasiliev, K. Alameh and M. Nur-E-Alam, *Appl. Sci.*, 2018, **8**, 849.
21 A. Arrigo, A. M. Cancelliere, M. Galletta, A. Burtone, G. Lanteri, F. Nastasi and F. Puntoriero, *Mater. Adv.*, 2023, **4**, 5200–5205.
22 I. Papakonstantinou, M. Portnoi and M. G. Debije, *Adv. Energy Mater.*, 2021, **11**, 2002883.
23 A. Albrecht, D. Pfennig, J. Nowak, M. Grunwald and P. J. Walla, *Nano Sel.*, 2020, **1**, 525–538.
24 M. M. Willich, L. Wegener, J. Vornweg, M. Hohgardt, J. Nowak, M. Wolter, C. R. Jacob and P. J. Walla, *Proc. Natl. Acad. Sci. U. S. A.*, 2020, **117**, 32929–32938.
25 A. Pieper, M. Hohgardt, M. Willich, D. A. Gacek, N. Hafi, D. Pfennig, A. Albrecht and P. J. Walla, *Nat. Commun.*, 2018, **9**, 666.
26 R. Mazzaro and A. Vomiero, *Adv. Energy Mater.*, 2018, **8**, 1801903.
27 K. Wu, H. Li and V. I. Klimov, *Nat. Photon.*, 2018, **12**, 105–110.
28 K. Kim, S. K. Nam, J. Cho and J. H. Moon, *Nanoscale*, 2020, **12**, 12426–12431.
29 S. Castelletto and A. Boretti, *Nano Energy*, 2023, **109**, 108269.
30 V. Balzani, P. Ceroni and A. Juris, *Photochemistry and Photophysics: Concepts, Research, Perspectives*, Wiley-VCH, Weinheim, 2014.
31 B. A. Swartz, T. Cole and A. H. Zewail, *Opt. Lett.*, 1977, **1**, 73–75.
32 C. Tummeltshammer, M. Portnoi, S. A. Mitchell, A.-T. Lee, A. J. Kenyon, A. B. Tabor and I. Papakonstantinou, *Nano Energy*, 2017, **32**, 263–270.
33 N. J. L. K. Davis, R. W. MacQueen, D. A. Roberts, A. Danos, S. Dehn, S. Perrier and T. W. Schmidt, *J. Mater. Chem. C*, 2016, **4**, 8270–8275.
34 J. t. Schiphorst, A. M. Kendhale, M. G. Debije, C. Menelaou, L. M. Herz and A. P. H. J. Schenning, *Chem. Mater.*, 2014, **26**, 3876–3878.
35 G. D. Gutierrez, I. Coropceanu, M. G. Bawendi and T. M. Swager, *Adv. Mater.*, 2016, **28**, 497–501.
36 B. Zhang, G. Lyu, E. A. Kelly and R. C. Evans, *Adv. Sci.*, 2022, **9**, 2201160.
37 C. Tummeltshammer, A. Taylor, A. J. Kenyon and I. Papakonstantinou, *J. Appl. Phys.*, 2014, **116**, 173103.
38 B. Balaban, S. Doshay, M. Osborn, Y. Rodriguez and S. A. Carter, *J. Lumin.*, 2014, **146**, 256–262.
39 J. Graffion, X. Catto, M. Wong Chi Man, V. R. Fernandes, P. S. Andre, R. A. S. Ferreira and L. D. Carlos, *Chem. Mater.*, 2011, **23**, 4773–4782.
40 B. Matarranz and G. Fernández, *Chem. Phys. Rev.*, 2021, **2**, 041304.
41 F. Nastasi, P. G. Mineo, J. Barichello, G. La Ganga, G. Di Marco, G. Calogero and M. Cordaro, *Biomimetics*, 2022, **7**, 110.
42 R. Ziessel, G. Ulrich and A. Harriman, *New J. Chem.*, 2007, **31**, 496–501.
43 M. Trapani, M. A. Castriciano, E. Collini, G. Bella and M. Cordaro, *Org. Biomol. Chem.*, 2021, **19**, 8118–8127.
44 M. Trapani, M. A. Castriciano, J. A. A. W. Elemans, P. Mineo, A. Nicosia and M. Cordaro, *Synlett*, 2021, **32**, 1714–1718.
45 M. Cordaro, P. Mineo, F. Nastasi and G. Magazzù, *RSC Adv.*, 2014, **4**(83), 43931–43933.
46 O. A. Bozdemir, S. Erbas-Cakmak, O. O. Eki, A. Dana and E. U. Akkaya, *Angew. Chem.*, 2011, **123**, 11099–11104.
47 N. J. L. K. Davis, R. W. MacQueen, D. A. Roberts, A. Danos, S. Dehn, S. Perrier and T. W. Schmidt, *J. Mater. Chem. C*, 2016, **4**, 8270–8275.
48 A. Vazquez-Romero, N. Kielland, M. J. Arevalo, S. Preciado, R. J. Mellanby, J. Richard, Y. Feng, R. Lavilla and M. Vendrell, *J. Am. Chem. Soc.*, 2013, **135**, 16018–16021.
49 M. Fakis, J. S. Beckwith, K. Seintis, E. Martinou, C. Nançoz, N. Karakostas, I. Petsalakis, G. Pistolis and E. Vauthey, *Phys. Chem. Chem. Phys.*, 2018, **20**, 837–849.
50 P. Porcu, I. González-Méndez, K. Sorroza-Martínez, A. S. Estrada-Montaño, F. Cuétara-Guadarrama, M. Vonlanthen and E. Rivera, *Dyes Pigm.*, 2022, **207**, 110713.
51 S. T. Bailey, G. E. Lokey, M. S. Hanes, J. D. M. Shearer, J. B. McLafferty, G. T. Beaumont, T. T. Baseler, J. M. Layhue, D. R. Broussard, Y.-Z. Zhang and B. P. Wittmershaus, *Sol. Energy Mater. Sol. Cells*, 2007, **91**, 67–75.
52 V. Balzani and F. Scandola, *Supramolecular Photochemistry*, Horwood, Chichester, 1991.
53 B. Zhang, C. Gao, H. Soleimaninejad, J. M. White, T. A. Smith, D. J. Jones, K. P. Ghiggino and W. W. H. Wong, *Chem. Mater.*, 2019, **31**, 3001–3008.
54 (*a*) R. Mazzaro, A. Gradone, S. Angeloni, G. Morselli, P. G. Cozzi, F. Romano, A. Vomiero and P. Ceroni, *ACS Photonics*, 2019, **6**, 2303–2311; (*b*) J. Bomm, A. Büchtemann, A. Fiore, L. Manna, J. H. Nelson, D. Hill and W. G. J. H. M. van Sark, *Beilstein J. Nanotechnol.*, 2010,

1, 94–100; (*c*) I. Coropceanu and M. G. Bawendi, *Nano Lett.*, 2014, **14**, 4097–4101.
55 F. Meinardi, F. Bruni and S. Brovelli, *Nat. Rev. Mater.*, 2017, **2**, 17072.
56 Average visible transmission (AVT), color rendering index (CRI) and color coordinates (LAB) have been calculated by using the calculator provided in the ESI† of the article: C. Yang, D. Liu, M. Bates, M. C. Barr and R. R. Lunt, How to Accurately Test, Characterize, and Report Transparent Solar Cells, *Joule*, 2019, **3**, 1803–1809.
57 R. Dabestani and I. N. Ivanov, *Photochem. Photobiol.*, 1999, **70**, 10–34.
58 N. J. Turro, *Modern Molecular Photochemistry*, Benjamin Cummings, Manlo Park, CA, 1978.
59 A. Arrigo, F. Nastasi, G. La Ganga, F. Puntoriero, G. Zappalà, A. Licciardello, M. Cavazzini, S. Quici and S. Campagna, *Chem. Phys. Lett.*, 2017, **683**, 96–104.
60 Y. Zhou, D. Benetti, X. Tong, L. Jin, Z. M. Wang, D. Ma, H. Zhao and F. Rosei, *Nano Energy*, 2018, **44**, 378–387.
61 F. Purcell-Milton and Y. K. Gun'ko, *J. Mater. Chem.*, 2012, **22**, 16687.
62 (*a*) C. Yang, *et al.*, *Joule*, 2022, **6**(1), 8–15; (*b*) M. G. Debije, R. C. Evans and G. Griffini, *Energy Environ. Sci.*, 2021, **14**, 293–301.
63 H. Zhao, D. Benetti, L. Jin, Y. Zhou, F. Rosei and A. Vomiero, *Small*, 2016, **12**, 5368.
64 Y. Zhou, D. Benetti, Z. Fan, H. Zhao, D. Ma, A. O. Govorov, A. Vomiero and F. Rosei, *Adv. Energy Mater.*, 2016, **6**, 1501913.
65 M. Aghaei, R. Pelosi, W. W. H. Wong, T. Schmidt, M. G. Debije and A. H. M. E. Reinders, *Prog. Photovoltaics*, 2022, **30**, 726–739.
66 G. Griffini, M. Levi and S. Turri, *Renewable Energy*, 2015, **78**, 288–294.
67 J. Roncali, *Adv. Energy Mater.*, 2020, **10**, 2001907.
68 Y. Wang, X. Shi, T. Oshikiri, S. Zu, K. Ueno and H. Misawa, *Nanoscale*, 2020, **12**, 22674–22679.
69 Z. Chen, *et al.*, *J. Mater. Res.*, 2010, **25**, 3.
70 R. E. Adam, M. Pirhashemib, S. Elhag, X. Liuc, A. Habibi-Yangjehb, M. Willandera and O. Nur, *RSC Adv.*, 2019, **9**, 8271–8279.
71 D. Ogermann, T. Wilke and K. Kleinermanns, *Open J. Phys. Chem.*, 2012, **2**, 47–57.
72 J. L. Banal, K. P. Ghiggino and W. W. H. Wong, *Phys. Chem. Chem. Phys.*, 2014, **16**, 25358.

